

# Possibility of increasing the efficiency of laser-induced tattoo removal by optical skin clearing

E.A. Genina, A.N. Bashkatov, V.V. Tuchin, G.B. Altshuler, I.V. Yaroslavski

**Abstract.** The possibility of selective laser photothermolysis improvement for the removal of tattoo pigments due to the optical clearing of human skin is investigated. It is shown experimentally that the optical skin clearing increases the tattoo image contrast. Computer Monte Carlo simulations show that by decreasing the laser beam scattering in upper skin layers, it is possible to reduce the radiation power required for tattoo removal by 30%–40% and, therefore, to increase the photothermolysis efficiency.

**Keywords:** laser photothermolysis, Monte Carlo simulation, immersion optical clearing, skin, tattoo.

## 1. Introduction

The problem of tattoo removal is as old as tattooing. In many cosmetic clinics the destructive methods of tattoo removal such as dermabrasion and argon or CO<sub>2</sub> laser vaporisation of upper skin layers are still widely used [1–3], but they have a high risk of scarring. The method of tattoo pigment removal by using selective laser thermolysis is efficient and safe enough [4–6]. Because of a variety of tattoo ink colours, different laser wavelengths are necessary. Nanosecond (10–100 ns) pulsed lasers emitting in the red and near-IR regions such as a 694-nm ruby laser [4–9] and Q-switched lasers, for example Nd:YAG (1064 and 532 nm) [5–9] and alexandrite (700–850 nm) [6, 9–11] lasers are most often used.

Pigmented ink particles used for tattoo are located

within dermal fibroblasts and mast cells, predominantly in a perivascular region [12]. Red and NIR laser radiation penetrates deeply enough into skin and it is absorbed strongly by blue, green, and black tattoo pigments included in the composition of the most tattoos [6]. Upon irradiation of skin by short laser pulses the heating and thermal destruction of pigment particles occur considerably quicker than the heating of surrounding dermal tissue [9, 10]. The destruction of ink particles and cells containing them, allows organism to remove the pigments by means of normal physiology with the help of lymphatic transport [13, 14].

The number of laser therapy sessions depends on the type of ink, the depth of tattoo location and the type of a laser. For some tattoos, deep pigmented layers may be screened by superficial ones, which requires multiple laser treatments [15, 16]. An additional difficulty appears because some multicolour tattoos contain pigments, that slightly absorb NIR radiation [14, 17]. Although, short-wavelength radiation is well absorbed by tattoo pigments, the use of visible lasers is limited by high light scattering in skin and in absorption hemoglobin [6], whereas an increase in the laser radiation intensity to compensate for energy losses caused by light scattering and absorption in tissue can damage the tissue itself, including a stable pigmentation of skin.

The optical immersion of skin based on the matching of the refractive indices of scattering centers (collagen and elastin fibers) and the surrounding substance (interstitial fluid) can improve laser tattoo removal because exogenous immersion agents have a higher refractive index than that of interstitial fluid. It is obvious that immersion, which reduces light scattering in skin, will improve the laser light delivery to the embedded ink particles and will allow the use of visible laser radiation, which can more efficiently act on some dyes.

In this paper, we studied immersion skin clearing for the enhancement of laser radiation absorption by tattoo pigments and other absorbing materials or pathological neoplasms lying at some depth in skin, for their destruction by selective laser thermolysis.

## 2. Materials and methods

### 2.1 Experimental investigation

Samples of human skin *in vitro* obtained post-surgically were studied. The mean area of the sample surface was about 20 × 30 mm. The adipose layer was removed. The thickness of samples was measured with an accuracy of ±50 μm by using a micrometer.

E.A. Genina, A.N. Bashkatov Scientific and Educational Institute of Optics and Biophotonics, N.G. Chernyshevsky Saratov State University, ul. Astrakhanskaya 83, 410012 Saratov, Russia; e-mail: eagenina@optics.sgu.ru, a.n.bashkatov@mail.ru;

V.V. Tuchin Scientific and Educational Institute of Optics and Biophotonics, N.G. Chernyshevsky Saratov State University, ul. Astrakhanskaya 83, 410012 Saratov, Russia; Institute for Problems of Precise Mechanics and Control, Russian Academy of Sciences, ul. Rabochaya 24, 410028 Saratov, Russia; e-mail: tuchin@sgu.ru;

G.B. Altshuler Palomar Medical Technologies, Burlington, MA, USA;

I.V. Yaroslavski Scientific and Educational Institute of Optics and Biophotonics, N.G. Chernyshevsky Saratov State University, ul. Astrakhanskaya 83, 410012 Saratov, Russia; present address: Palomar Medical Technologies, Burlington, MA, USA

Received 20 February 2008

Kvantovaya Elektronika 38 (6) 580–587 (2008)

Translated by E.A. Genina

Both blue and black inks were used for tattooing. The inks were injected into the back side of a skin sample up to depth 0.2–0.3 mm by a special needle for tattooing. Thus, for the skin sample thickness  $\sim 0.6$  mm, the depth of tattoo location was 0.3–0.4 mm. Figure 1 presents the absorption spectra of diluted ink solutions recorded with a LESA-5 optical multichannel analyser ('BioSpec', Russia). One can see that the absorption coefficient of the black ink has not any maxima and decreases monotonically with increasing the wavelength. The absorption bands of the blue ink had maxima at 630 and 716 nm. The concentrations of the black and blue inks were  $0.25 \mu\text{L mL}^{-1}$  (0.025 %) and  $0.312 \mu\text{L mL}^{-1}$  (0.0312 %), respectively.

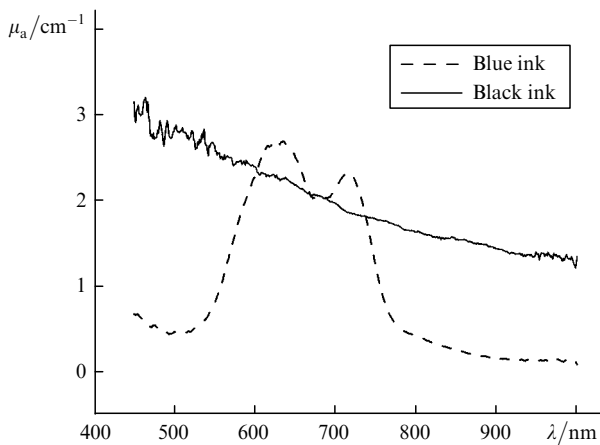


**Figure 1.** Spectral dependence of the absorption coefficient of aqueous dye solutions used for tattoo: the solid curve corresponds to the black dye and the dashed curve corresponds to the blue dye; dye concentrations in the solutions are:  $0.25 \mu\text{L mL}^{-1}$  for the black dye and  $0.312 \mu\text{L mL}^{-1}$  for the blue dye.

The immersion agent was the aqueous solution of glycerol with concentration 88 % ('Ecolab', Russia). The refractive index of the solution measured with an IRF-454B2M refractometer was 1.45.

To overcome a protective skin barrier, the method of producing microdamages in the epidermal stratum corneum described in detail in [18] was used. The thermal action produced microchannels of diameter  $200 \pm 20 \mu\text{m}$  and depth  $25 \pm 5 \mu\text{m}$  on the skin surface. The thermally-induced products were removed from the microchannels by treating the skin surface with the aqueous 40 % ethanol solution. This procedure also provided the increase in the stratum corneum permeability [19, 20], especially within the channels.

**Table 1.** Parameters of skin layers used in simulations [22].

Skin layers	Thickness/ $\mu\text{m}$	Refractive index	Water content (%)	Blood content (%)	Scattering coefficient of a bloodless tissue at 577 nm/ $\text{cm}^{-1}$	Mean vessel diameter/ $\mu\text{m}$
Epidermis (including stratum corneum)	100	1.45	60	0	300	–
Basal membrane	15	1.4	60	0	300	–
Derma with upper vessel plexus	200	1.38	75	1.7	120	6
Reticular dermis	1500	1.35	75	1.4	120	15
Derma with lower vessel plexus	200	1.38	75	1.7	120	6
Subcutaneous adipose layer	3000	1.44	5	0	130	–

The skin samples with tattoos and previously perforated stratum corneum were treated with the glycerol solution. The samples were fixed on a cell so that the immersion agent interacted only with the perforated area of the stratum corneum. The samples were photographed with a Coolpix 995 digital camera (Nikon, USA) before and 24 h after the start of the glycerol solution action. The experiments were performed at  $20^\circ\text{C}$ .

## 2.2 Monte Carlo simulation

The efficiency of laser radiation delivery to the areas of tattoo pigment localisation was estimated by using Monte Carlo simulations of variations in the optical properties of skin.

Skin is a complex heterogeneous structure consisting of three main layers: epidermis ( $\sim 100 \mu\text{m}$  thick), dermis ( $\sim 1 - 2$  mm thick), and subcutaneous adipose tissue ( $1 - 6$  mm thick) [21]. The optical properties of these layers are characterised by absorption  $\mu_a$  and scattering  $\mu_s$  coefficients, and anisotropy factor  $g$ , which is the average cosine of the scattering angle. The distribution of blood, water, melanin and other chromophores in skin produce variations in the optical properties of each layer. These variations allow subdividing each skin layer into sublayers. Epidermis is subdivided into two sublayers: stratum corneum ( $\sim 20\text{-}\mu\text{m}$  thick), which is composed of dry keratinised cellular remains, and living epidermis ( $\sim 100\text{-}\mu\text{m}$  thick) containing a main skin pigment – melanin. Derma is a main skin layer comprising blood; in turn, it can be subdivided into three main sublayers: dermis with upper blood net plexus ( $200\text{-}\mu\text{m}$  thick), reticular dermis ( $\sim 1.5\text{-mm}$  thick) and dermis with deep blood net plexus ( $200\text{-}\mu\text{m}$  thick). Between epidermis and dermis, a  $15\text{-}\mu\text{m}$ -thick basal membrane is located [21, 22].

The absorption properties of skin are mainly determined by absorption in melanin, water, and blood hemoglobin [23]. Scattering is determined by the fibrous structure of the tissue, i.e. by scattering from collagen fibrils of dermis and from mitochondria and nuclei of epidermal cells. In accordance with the optical and the structural-morphological properties of skin, we used the six-layer skin model with parameters presented in Table 1.

The visible and NIR absorption in each layer is determined by absorption in three main skin chromophores: blood, melanin and water. The absorption coefficients for each layer are described by the expression [22]:

$$\mu_{ak} = B_k C_k \mu_a^{\text{bl}}(\lambda) + (1 - B_k - W_k) \mu_a^{\text{bg}} + M_k \mu_a^{\text{mel}}(\lambda) + W_k \mu_a^{\text{wat}}(\lambda), \quad (1)$$

where  $k = 1, \dots, 6$  is the layer number;  $B_k$  and  $W_k$  are the volume fractions of blood and water in each layer; for the melanin containing layers (epidermis and basal membrane),  $M_k = 1$ , for the other skin layers,  $M_k = 0$ ;  $\mu_a^{\text{bl}}$ ,  $\mu_a^{\text{mel}}$ ,  $\mu_a^{\text{wat}}$ , and  $\mu_a^{\text{bg}}$  are the absorption coefficients of blood, melanin, water and the base substance (collagen) of tissue, respectively (within the framework of the model,  $\mu_a^{\text{bg}}$  is assumed to be wavelength independent and equal to  $0.15 \text{ cm}^{-1}$  [22]); and  $C_k$  is a correction factor. The correction factor is a number from 0 to 1 taking into account the fact that blood is localised in vessels rather than distributed homogeneously in the skin dermis. If the blood vessel diameter is large enough, and light does not penetrate inside the vessel, hemoglobin inside the vessel should not be taken into account as an absorber, and then, the correction factor will be considerably smaller than unity. Otherwise, the correction factor for thin vessels will tend to unity. Taking into account that the correction factor depends on the vessel diameter, we used in the model the empiric expression [24]:

$$C_k = \frac{1}{1 + a(0.5\mu_a^{\text{bl}}d_k^{\text{ves}})^b},$$

where  $d_k^{\text{ves}}$  is the blood vessel diameter in centimeters. If blood vessels lying parallel to the skin surface are illuminated by a collimated light beam,  $a = 1.007$  and  $b = 1.228$ , while for diffuse illumination of the vessels,  $a = 1.482$  and  $b = 1.151$ . The optical properties of blood (the anisotropy factor and absorption and scattering coefficients) were simulated by using the algorithm described in detail in [25]. We assumed that the degree of hemoglobin oxygenation was 0.8 (because the degree of oxygenation hemoglobin for arterial blood is 0.9 and that for venous blood is 0.7). The blood hematocrit is 0.4. The optical properties of water are well investigated at present; we used the data presented in Refs [26, 27].

The scattering coefficient of skin layers is described by the expression [22]:

$$\mu_{sk}(\lambda) = B_k C_k \mu_s^{\text{bl}}(\lambda) + (1 - B_k) \mu_{sk}^{\text{bg}}(\lambda). \quad (2)$$

Here

$$\mu_{sk}^{\text{bg}}(\lambda) = \mu_{sk}^0(577/\lambda) \quad (3)$$

is the scattering coefficient of the bloodless tissue [22];  $\mu_{sk}^0$  is the scattering coefficient of bloodless tissue at a wavelength of 577 nm (see Table 1); and  $\lambda$  is expressed in nanometers.

The anisotropy scattering factor is described by the expression [22]:

$$g_k(\lambda) = \frac{B_k C_k \mu_s^{\text{bl}}(\lambda) g^{\text{bl}} + (1 - B_k) \mu_{sk}^{\text{bg}}(\lambda) g^{\text{bg}}(\lambda)}{\mu_{sk}(\lambda)}, \quad (4)$$

where

$$g^{\text{bg}}(\lambda) = 0.7645 + 0.2355 \left[ 1 - \exp\left(-\frac{\lambda - 500}{729.1}\right) \right] \quad (5)$$

is the anisotropy scattering factor of the bloodless tissue [22]. The melanin absorption coefficient in the model is determined from the empirical expression [22]

$$\mu_a^{\text{mel}}(\lambda) = A \exp\left(-\frac{\lambda - 800}{182}\right), \quad (6)$$

where the parameter  $A$  is the ratio of the optical density of pigmented skin layers (epidermis and basal membrane) to their thickness. In our model,  $A = 0.87 \text{ cm}^{-1}$  for epidermis and  $13.5 \text{ cm}^{-1}$  for basal membrane [22].

The optical clearing of different skin layers was simulated by using the Mie scattering theory [28], which requires the knowledge of the refractive indices of skin scatterers and surrounding interstitial fluid, and also sizes of the scatterers. Calculations for epidermis and basal membrane were performed by using the model of spherical particles, while for dermis the model of cylindrical particles was used. The spherical scatterers were used to describe epidermis scattering properties because cell mitochondria are the main scatterers in epithelial tissues [29, 30]. Scattering in dermis was described by cylindrical scatterers due to the fibrous structure of dermis [30, 31]. Because the particle size distribution and the packing factor of scatterers are unknown, monodisperse so-called Mie-equivalent particles were used in simulations.

The scattering coefficient of the upper skin layers was calculated from the expression

$$\mu_s(\lambda) = \frac{3}{4} \frac{\varphi}{\pi a_{\text{sph}}^3} \pi a_{\text{sph}}^2 Q_s(a_{\text{sph}}, n_s, n_i) F(\lambda), \quad (7)$$

where  $a_{\text{sph}}$  is the radius of spherical scatterers;  $Q_s(a_{\text{sph}}, n_s, n_i)$  is the scattering efficiency factor;  $F(\lambda)$  is the packing factor of scatterers;  $n_s$  is the refractive index of scatterers;  $n_i$  is the refractive index of interstitial fluid; and  $\varphi$  is the volume fraction of scatterers for each layer. The scattering coefficient for dermis layers was calculated from the expression

$$\mu_s(\lambda) = \frac{\varphi}{\pi a_c^2} 2a_c Q_s(a_c, n_s, n_i) F(\lambda), \quad (8)$$

where  $a_c$  is the radius of cylindrical scatterers. The effective size of scatterers and the packing factor were calculated by minimising the target function

$$\text{TF}(a(\lambda), F(\lambda)) = (\mu_s^{\text{mod}} - \mu_s^{\text{Mie}})^2 + (g^{\text{mod}} - g^{\text{Mie}})^2. \quad (9)$$

Here,  $\mu_s^{\text{mod}}$  and  $g^{\text{mod}}$  correspond to the data calculated from Eqns (2)–(5) for each layer;  $\mu_s^{\text{Mie}}$  and  $g^{\text{Mie}}$  are the scattering coefficient [(Eqns (7) and (8))] and the anisotropy factor calculated for each layer by using the Mie theory. The target function was minimised by the simplex Nelder – Mead method described in detail in [32].

The influence of clearing agents on the optical properties of skin (diffuse reflectance and a fraction of light absorbed by a tissue) was simulated by replacing the interstitial fluid by the clearing agent (aqueous glycerol solution) with the refractive index higher than that of the interstitial fluid. Calculations were performed by assuming that the refractive index of the skin interstitial fluid is equal to that of water, and the refractive index of the aqueous glycerol solution is 1.45. It was assumed that the sizes of effective skin scatterers, the packing factor of the scatterers and the refractive index of the scatterers were invariable during the optical clearing.

Tattoo was simulated by adding a 50- $\mu\text{m}$ -thick absorbing layer in the form of a cross of size  $1 \times 1$  cm to the skin model. The area of the simulated skin sample was  $3 \times 3$  cm. It was assumed that the ink in this layer was undiluted [i.e. the absorption coefficient of the inks (see Fig. 1) was recalculated for concentration 100 %]. The depth of the absorbing layer in the model was set equal to 0.5 or 1 mm because the standard depth of ink injection at the tattooing with the help of mechanical devices is from 0.2 to 1 mm depending on the technology and equipment used [17].

The Monte Carlo (MC) simulation was performed by using the algorithm presented in [33]. The stochastic MC method is widely used to simulate the propagation of optical radiation in complex random highly scattering and absorbing media such as biological tissues. The MC simulation of photon packet trajectories was performed by simulating the sequence of elementary events: photon mean free path generation, scattering and absorption events, reflection or/and refraction on interfaces. The initial and final states of photons are entirely determined by the source and detector geometry. Reflection spectra were simulated and the fraction of photons absorbed in the tattoo area was calculated by representing the incident light in the form of a narrow beam normally incident on the tissue surface. In the simulation  $10^5$  photon packets were used. Reflection spectra were simulated by detecting all photons backscattered to the upper half-plane over the tissue surface. The specular reflection of photons from the air–tissue interface was separately taken into account.

The fraction of photons absorbed in the tattoo area was calculated in the following way: when the photon packet trajectory passed through the tattoo area, the parameter  $A_{\text{tat}}$  (the fraction of photons absorbed in the tattoo area) was increased by  $w\mu_a/(\mu_a + \mu_s)$  in the each interaction event [33], where  $w$  is the current weight of the photon packet, and  $\mu_a$  and  $\mu_s$  are the absorption and scattering coefficients at the given point, respectively. After the detection of all photon

packets, the value  $A_{\text{tat}}$  was summed over all packets and normalised to the total weight of packets used in simulations.

A new propagation direction of a scattered photon packet was determined according to the Henyey–Greenstein scattering phase function:

$$f_{\text{HG}}(\theta) = \frac{1}{4\pi} \frac{1 - g^2}{(1 + g^2 - 2g \cos \theta)^{3/2}},$$

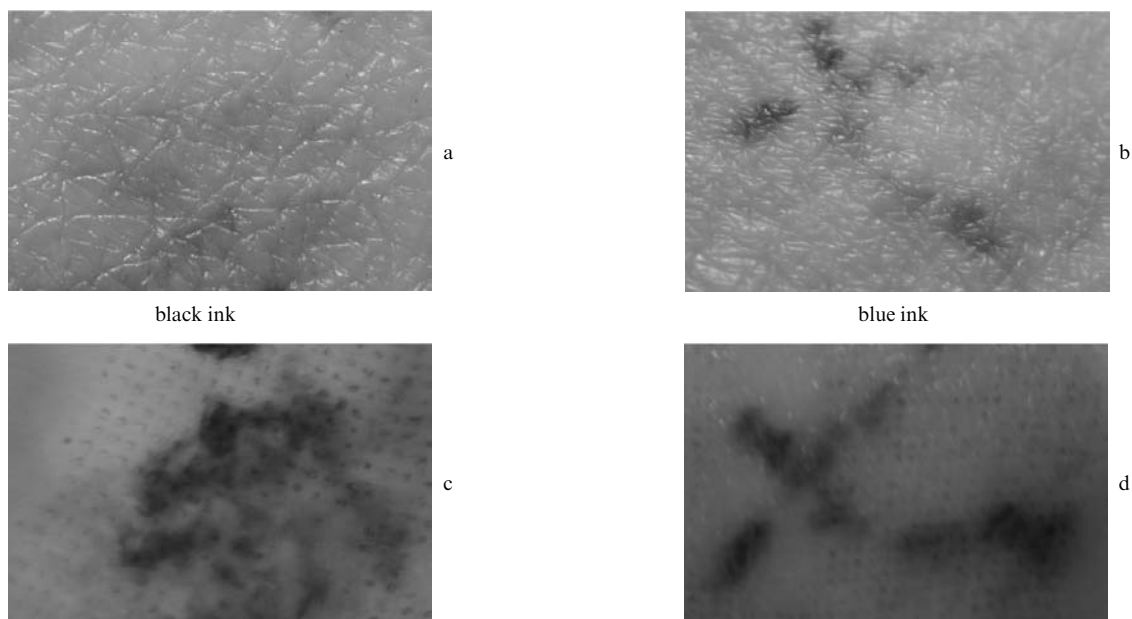
where  $\theta$  is the polar scattering angle. The distribution over the azimuthal scattering angle was assumed uniform.

Skin images with tattoo were simulated by using  $25 \times 10^6$  photon packets. Photons normally incident on the skin surface were uniformly distributed over the area  $3 \times 3$  cm. Backscattered photons were detected by dividing this area ( $3 \times 3$  cm) into cells of area  $0.01 \text{ mm}^2$ . The weight of a backscattered photon was recorded to the array cell corresponding to the coordinates of the photon exit point and, then was summed over all packets and normalised to the average weight of the photon packets incident on the correspondent area.

The thicknesses and refractive indices of skin layers used in MC simulations are presented in Table 1. Absorption coefficients for each wavelength and each layer were calculated from Eqn (1), and scattering coefficients and anisotropy factors of skin layers without optical clearing were calculated from Eqns (2)–(5). In the case of immersion clearing of skin, scattering coefficients and anisotropy factors of skin layers were calculated from Eqns (7) and (8) by using the Mie theory [28].

### 3. Results and discussion

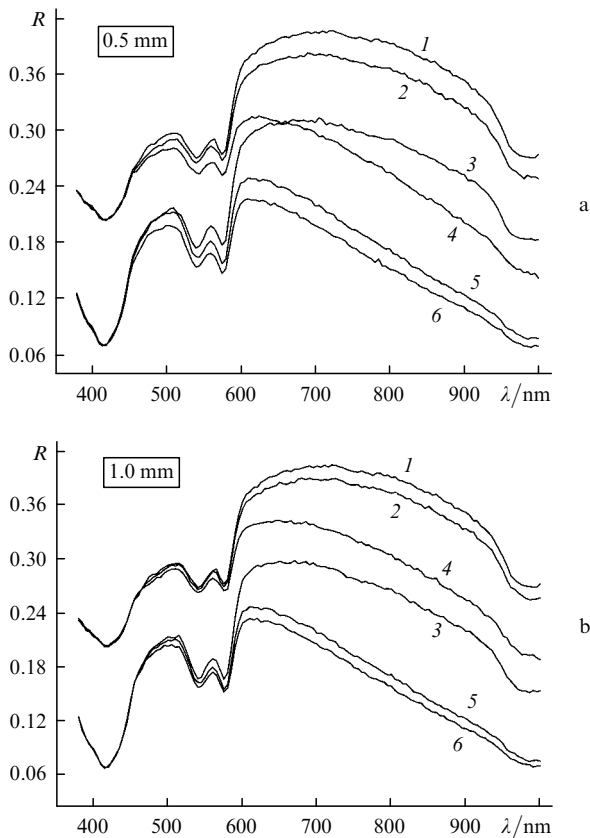
Figure 2 shows human skin samples with black and blue tattoo before and after the treatment with the aqueous glycerol solution for 24 hours. The epidermal corneous layer of both samples was previously perforated. One can see that at the initial moment (Fig. 2a, b) tattoo were



**Figure 2.** Images of skin surface with black ink tattoo (a, c) and blue ink tattoo (b, d); the sample with tattoo before glycerol action (a, b) and after microperforation of skin surface and glycerol action during 24 hours (c, d).

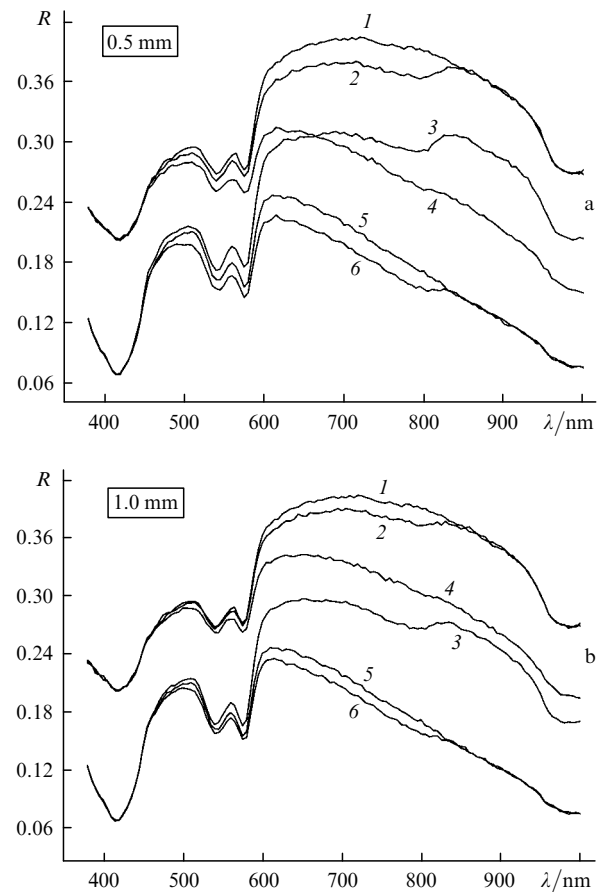
visualised significantly worse than after treatment and immersion (Figs 2c, d). In both cases, the thickness of samples decreased from  $0.6 \pm 0.05$  mm at the initial moment to  $0.5 \pm 0.05$  mm after the treatment with the glycerol solution.

Figure 3 presents the reflection spectra of skin calculated by the MC method at different conditions. Curve (1) shows the reflection spectrum of the intact skin without tattoo. Curve (2) corresponds to the reflection spectrum of skin without clearing and with black tattoo located at the depth of 0.5 (Fig. 3a) and 1.0 mm (Fig. 3b). Curves (3) and (4) correspond to the cases when skin layers over or under tattoo are immersed. Curves (5) and (6) are the reflection spectra of totally immersed skin without/with tattoo, respectively. In all cases the subcutaneous adipose layer was not immersed. Figure 4 presents the diffuse reflection of skin simulated without/with blue tattoo at the depth of 0.5 and 1 mm, respectively.



**Figure 3.** Result of MC simulation of skin reflectance with black tattoo at a depth of 0.5 (a) or 1.0 mm (b): skin without both tattoo and clearing (1); skin with tattoo and without clearing (2); skin layers lying above tattoo are immersed (3); skin layers lying under tattoo (excluding subcutaneous adipose layer) are immersed (4); skin without tattoo, all layers (excluding subcutaneous adipose layer) are immersed (5); skin with tattoo, all layers (excluding subcutaneous adipose layer) are immersed (6).

Curves (1) and (5) in Figs 3 and 4 coincide because they correspond to skin without tattoo and without immersion or totally immersed, respectively. The shape of the spectra is determined by absorption of melanin, the absorption bands of blood hemoglobin at 416, 542 and 575 nm [25], and water at 980 nm [26], and also by the scattering spectrum of skin.



**Figure 4.** Result of MC simulation of skin reflectance with blue tattoo at a depth of 0.5 (a) or 1.0 mm (b): skin without both tattoo and clearing (1); skin with tattoo and without clearing (2); skin layers lying above tattoo are immersed (3); skin layers lying under tattoo (excluding subcutaneous adipose layer) are immersed (4); skin without tattoo, all layers (excluding subcutaneous adipose layer) are immersed (5); skin with tattoo, all layers (excluding subcutaneous adipose layer) are immersed (6).

The absorption spectra of dyes affect the shape of the reflection spectrum of skin. The presence of tattoo reduces the skin reflectance due to absorption of light by pigments in the ink. One can see that at the decrease of pigment location depth the skin reflectance decreases more significantly.

Monte Carlo simulations of skin images with black or blue ink tattoo localised under the skin layer at a depth of 0.5 and 1 mm are presented in Figs 5a–d and Fig. 5e–h, respectively. The images were constructed by using the optical parameters of skin calculated at 633 nm. Because the absorption coefficients of black and blue dyes at this wavelength and at this concentration virtually coincide, the images of tattoo in Fig. 5 can be assigned to both dyes.

The tattoo borders in Fig. 5 look rather blurred [it is especially visible in the images of deep tattoos ( $\sim 1$  mm)] (see Figs 5e–h), due to strong light scattering by upper tissue layers. The optical clearing of these layers significantly enhances the image contrast which improves the tattoo localisation and visualisation. The image contrast was estimated by the expression  $K = (R_1 - R_2)(R_1 + R_2)^{-1}$ , where  $R_1$ ,  $R_2$  are the skin reflectances outside the tattoo and within it, respectively. The image contrast of tattoo located at a depth of 0.5 mm against the background of intact skin is  $= 0.33$ . When skin was completely immersed,

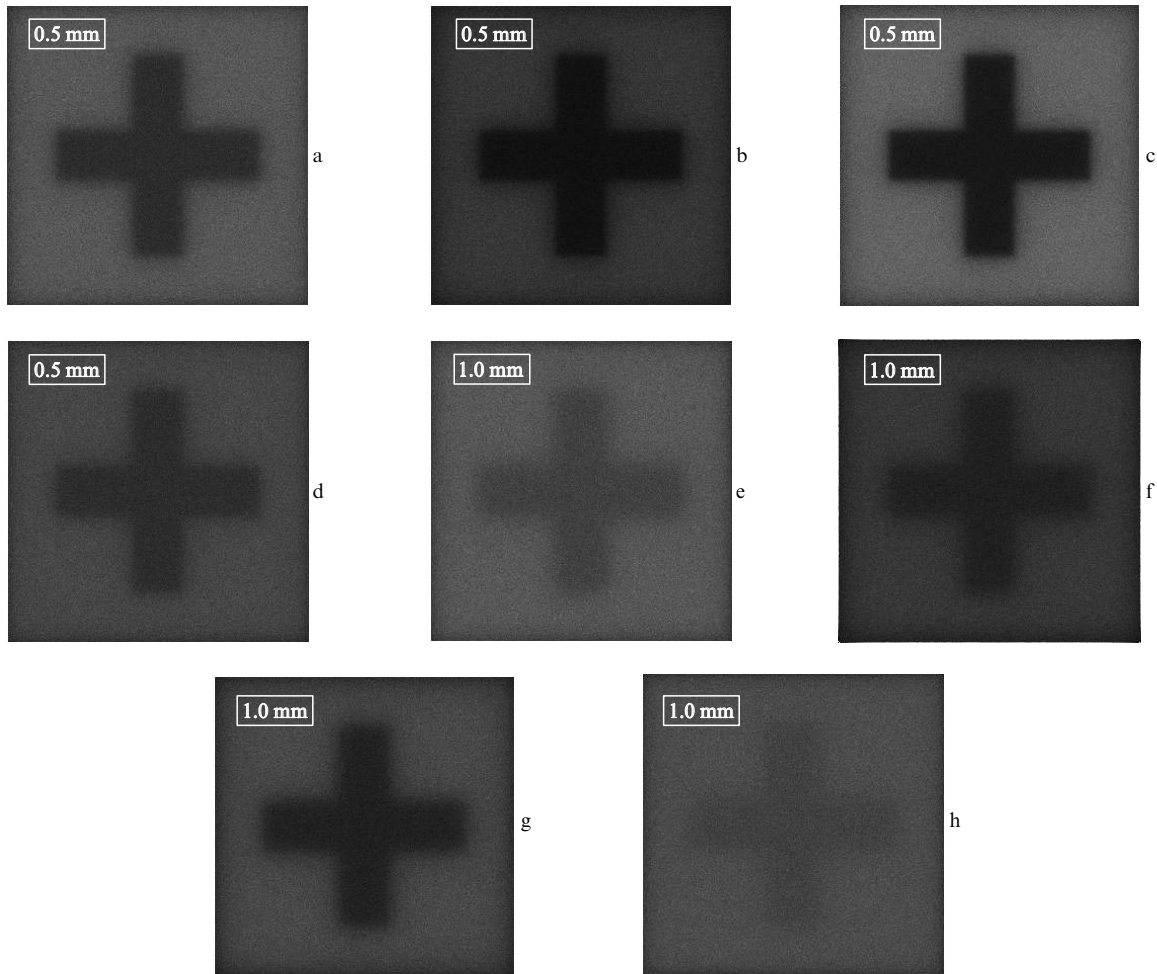


**Figure 5.** Result of MC simulation of skin tattoo image in reflected light (reflectance) at wavelength 633 nm, the depth of tattoo is 0.5 and 1.0 mm, the size of tattoo is  $1 \times 1$  cm, the area of the simulated skin sample is  $3 \times 3$  cm: skin without clearing (a, e); all skin layers (excluding subcutaneous adipose layer) are immersed (b, f); skin layers lying above the tattoo are immersed by the agent administering topically (c, g); skin layers lying under the tattoo are immersed by injection of the agent (d, h).

the contrast increased approximately by a factor of 1.5 ( $K = 0.5$ ). When only the upper skin layers were cleared (before tattoo) the contrast increased almost twice ( $K = 0.63$ ), whereas when only the lower skin layers were cleared, the contrast decreased by 1.7 times ( $K = 0.2$ ). The analysis of the image of tattoo located at a depth of 1 mm shows that the largest contrast is also achieved upon clearing the upper layer ( $K = 0.4$ ), which exceeds the tattoo image contrast against the intact skin background by a factor of 2.6 ( $K = 0.15$ ). A weak increase in the contrast is observed when skin is totally immersed ( $K = 0.28$ ). The contrast decreases if only lower skin layers are cleared ( $K = 0.09$ ). Thus, Fig. 5 shows that the clearing of epidermis and upper dermis layers is preferable because in this case the image contrast is maximal.

Figures 6 and 7 present the spectral dependences of the fraction of photons absorbed in the area of black and blue tattoo at depths of 0.5 and 1 mm. Curves (1) and (5) in these figures, which correspond to intact and totally immersed skin without tattoo, coincided. One can see that the sample without tattoo almost does not absorb in the spectral range under study. The presence of tattoo changes the spectral dependence of the fraction of absorbed photons in accordance with the absorption spectrum of the

dye used. The simulation of propagation of photons in skin showed that the immersion of layers under tattoo reduces the number of photons absorbed in the given area, which is well seen in Figs 5b, d and f, h. This is explained by the fact that photons that have passed through upper skin layers and the stained layer to the weakly scattering area propagate through this area without changing their propagation direction and are absorbed in deeper skin layers. Thus, they cannot make the contribution to the photon fraction absorbed in the tattoo area. At the same time, when only upper layers lying over the stained layer are cleared, a significant number of photons propagate through the upper layers almost without scattering and are absorbed in the stained layer. In this case, photons that have passed through the absorbing layer to the area under the tattoo can after the scattering in lower layers return into the stained layer and be absorbed there. Thus, the clearing of upper skin layers allows one to reduce significantly the laser power used for thermolysis by increasing light absorption in tattoo. The fraction of photons absorbed in the region from 600 to 1000 nm increases upon clearing upper skin layers on average by 30% and 40% for tattoos at depths of 0.5 and 1 mm, respectively. Thus, for deeply located tattoo this method of clearing is most efficient.

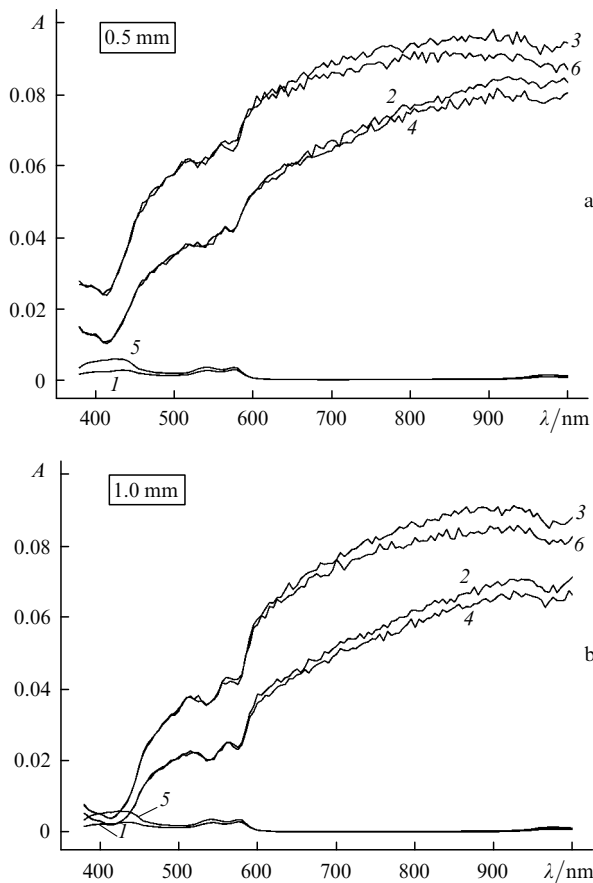


**Figure 6.** Result of MC simulation of absorbed photon fraction in skin (in the black tattoo area) at a depth of 0.5 (a) or 1.0 mm (b) under the different conditions: skin without both tattoo and clearing (1); skin with tattoo and without clearing (2); skin layers lying above tattoo are immersed (3); skin layers lying under tattoo (excluding subcutaneous adipose layer) are immersed (4); skin without tattoo, all layers (excluding subcutaneous adipose layer) are immersed (5); skin with tattoo, all layers (excluding subcutaneous adipose layer) are immersed (6).

We estimate the laser power density used in photothermolysis from the data presented in the literature. In particular, the energy density of a 755-nm alexandrite laser is  $5 \text{ J cm}^{-2}$  [6]. It follows from the data presented in Figs 6 and 7 that in the area of tattoo localisation at depths of 0.5 and 1 mm the absorbed light fraction is 0.07 and 0.05, which corresponds to  $0.35$  and  $0.25 \text{ J cm}^{-2}$ , respectively. In the case of clearing, the fraction of absorbed photons increases up to 0.09 and 0.07 for the depths of 0.5 and 1 mm, and energy density absorbed by the tattoo pigments increases up to  $0.45$  and  $0.35 \text{ J cm}^{-2}$ , respectively. Thus, to achieve the same result, which can be obtained without skin optical clearing, the laser energy density can be decreased by 30%–40% depending on the tattoo localisation depth.

The results obtained in the study have shown that the immersion of upper skin dermis layers significantly increases the fraction of photons absorbed by the dyes. The microperforation of the epidermal stratum corneum, which causes the efficient immersion of upper skin layers over tattoo not only accelerates skin clearing process due to the formation of channels in epidermis as shown in [18, 21, 34–36], but provides an increase in the fraction of light absorbed in the tattoo area. The injection of an immersing agent into skin

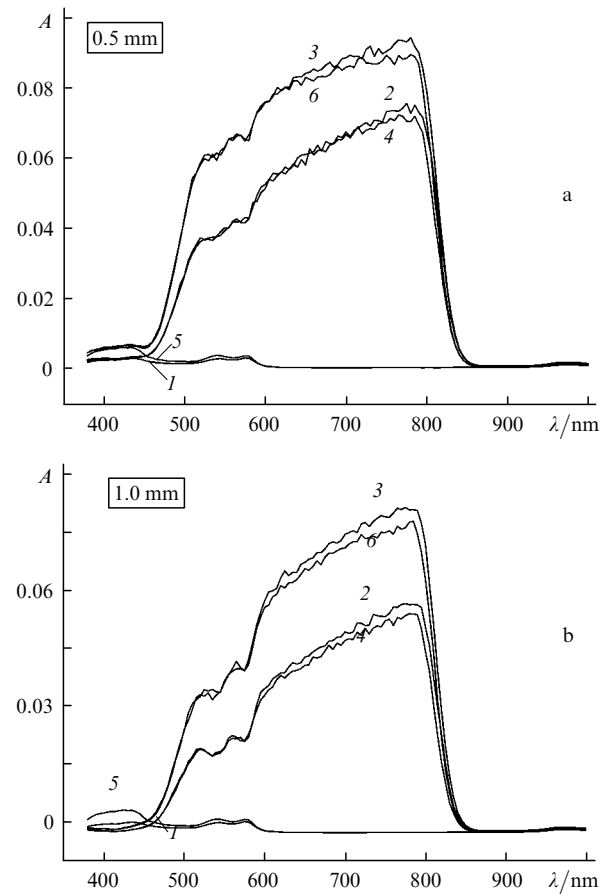


**Figure 7.** Result of MC simulation of absorbed photon fraction in skin (in the blue tattoo area) at a depth of 0.5 (a) or 1.0 mm (b) under the different conditions: skin without both tattoo and clearing (1); skin with tattoo and without clearing (2); skin layers lying above tattoo are immersed (3); skin layers lying under tattoo (excluding subcutaneous adipose layer) are immersed (4); skin without tattoo, all layers (excluding subcutaneous adipose layer) are immersed (5); skin with tattoo, all layers (excluding subcutaneous adipose layer) are immersed (6).

dermis under tattoo is less efficient because it reduces the fraction of absorbed photons in the tattoo area.

#### 4. Conclusions

We have studied immersion optical clearing of different skin layers containing dyes imitating tattoo. The images of skin with tattoo located at different depths in dermis have been constructed by using Monte Carlo simulations. It has been shown that upon clearing upper skin layers, the photon fraction absorbed in tattoo areas at the depths of 0.5 or 1 mm increases on average by 30% or 40%, which allows a significant decrease in the power of laser radiation used in thermolysis.

**Acknowledgements.** The study was supported by Palomar Medical Technologies Inc. (Burlington, USA), the Russian Federal Agency of Education of Russian Federation (Grant Nos 1.4.06 and RNP.2.1.1.4473) and partially by the Russian Foundation for Basic Research (Grant No. 06-02-16740).

## References

1. Scutt R.W.B. *Br. J. Plast. Surg.*, **25**, 189 (1972).
2. Reid R., Muller S. *Plast. Reconstr. Surg.*, **65**, 717 (1980).
3. Apfelberg D.B., Maser M.R., Lash H., White D.N., Flores J.T. *Ann. Plast. Surg.*, **14**, 6 (1985).
4. Huzaira M., Anderson R. *Lasers Surg. Med.*, **31**, 121 (2002).
5. Levine V.J., Geronemus R.G. *Cutis*, **55**, 291 (1995).
6. McNichols R.J., Fox M.A., Gowda A., Tuya S., Bell B., Motamedi M. *Lasers Surg. Med.*, **36**, 289 (2005).
7. Kilmer S.L., Anderson R.R. *J. Dermatol. Surg. Oncol.*, **19**, 330 (1993).
8. Fitzpatrick R.E., Lupton J.R. *Lasers Surg. Med.*, **27**, 358 (2000).
9. Leuenberger M.L., Mullas M.W., Hata T.R., Goldman M.P., Fitzpatrick R.E., Grevelink J.M. *Dermatol. Surg.*, **25**, 10 (1999).
10. Alster T.S. *J. Am. Acad. Dermatol.*, **33**, 69 (1995).
11. Moreno-Arias G.A., Casals-Andreu M., Camps-Fresneda A. *Lasers Surg. Med.*, **25**, 445 (1999).
12. Mann R., Klingmuller G. *Arch. Dermatol. Res.*, **271**, 367 (1981).
13. Fergusson J.E., Andrew S.M., Jones C.J., August P.J. *Br. J. Dermatol.*, **137**, 405 (1997).
14. Timko A.L., Miller C.H., Johnson F.B., Ross E.V. *Arch. Dermatol.*, **137**, 143 (2001).
15. Alster T.S. *J. Am. Acad. Dermatol.*, **33**, 69 (1995).
16. Dozier S.E., Diven D.G., Jones D., Brysk M., Sanchez R.L., Motamedi M. *Dermatol. Surg.*, **21**, 237 (1995).
17. Zelickson B.D., Mehregan D.A., Zarrin A.A., Coles C., Hartwig P., Olson S., Leaf-Davis J. *Lasers Surg. Med.*, **15**, 364 (1994).
18. Genina E.A., Bashkatov A.N., Korobko A.A., Zubkova E.A., Tuchin V.V., Yaroslavsky I.V., Altshuler G.B. *J. Biomed. Opt.*, **13**, 021102 (2008).
19. Peck K.D., Ghanem A.-H., Higuchi W.I. *Pharmaceutical Res.*, **11**, 1306 (1994).
20. Genina E.A., Bashkatov A.N., Tuchin V.V. *Medical Laser Application*, **23**, 31 (2008).
21. Schaefer H., Redelmeier T.E. *Skin barrier: Principles of Percutaneous Absorption* (Basel: Karger, 1996).
22. Altshuler G., Smirnov M., Yaroslavsky I. *J. Phys. D: Appl. Phys.*, **38**, 2732 (2005).
23. Meglinski I.V. *Kvantovaya Elektron.*, **31**, 1101 (2001) [*Quantum Electron.*, **31**, 1101 (2001)].
24. Bashkatov A.N., Tuchin V.V., Genina E.A., Stolnitz M.M., Zhestkov D.M., Altshuler G.B., Yaroslavsky I.V. *Proc. SPIE Int. Soc. Opt. Eng.*, **6436**, 64360Z (2007).
25. Bashkatov A.N., Zhestkov D.M., Genina E.A., Tuchin V.V. *Opt. Spektrosk.*, **98**, 695 (2005).
26. Hale G., Querry M.R. *Appl. Opt.*, **12**, 555 (1973).
27. Smith R.C., Baker K.S. *Appl. Opt.*, **20**, 177 (1981).
28. Bohren C.F., Huffman D.R. *Absorption and Scattering of Light by Small Particles* (New York: Wiley, 1983).
29. Mourant J.R., Freyer J.P., Hielscher A.H., Eick A.A., Shen D., Johnson T.M. *Appl. Opt.*, **37**, 3586 (1998).
30. Tuchin V.V. *Tissue Optics: Light Scattering and Instruments for Medical Diagnostics* (Bellingham, WA: SPIE Press, 2007) Vol. PM 166.
31. Saidi I.S., Jacques S.L., Tittel F.K. *Appl. Opt.*, **34**, 7410 (1995).
32. Bunday B. *Basic Optimization Methods* (London: Edward Arnold, 1984).
33. Wang L., Jacques S.L., Zheng L. *Comp. Methods Progr. Biomed.*, **47**, 131 (1995).
34. Tuchin V.V., Altshuler G.B., Gavrilova A.A., Pravdin A.B., Tabatadze D., Childs J., Yaroslavsky I.V. *Lasers Surg. Med.*, **38**, 824 (2006).
35. Genina E.A., Bashkatov A.N., Gavrilova A.A., Pravdin A.B., Tuchin V.V., Yaroslavsky I.V., Altshuler G.B. *Proc. SPIE Int. Soc. Opt. Eng.*, **6734**, 673419 (2007).
36. Altshuler G.B., Bashkatov A.N., Genina E.A., Gavrilova A.A., Pravdin A.B., Tabatadze D., Childs J., Yaroslavsky I.V., Tuchin V.V. *Lasers Surg. Med., Suppl.*, **18**, 2 (2006).